Experimental Eye Research xxx (2010) 1–6

Contents lists available at ScienceDirect

Experimental Eye Research

journal homepage: www.elsevier.com/locate/yexer

Development of a novel instrument to measure the pulsatile movement of ocular tissues☆

K. Singh [a,d,1], C. Dion [a,d,1], S. Costantino [b,c,d], M. Wajszilber [d], M.R. Lesk [b,d], T. Ozaki [a,d,*]

[a] Institut National de la Recherche Scientifique, Énergie, Matériaux et Télécommunications, Varennes, Québec J3X 1S2, Canada
[b] Département d'Ophtalmologie, Faculté de Médecine, Université de Montréal, Montréal, Québec H3T 1J4, Canada
[c] Institut de Génie Biomédical, Faculté de Médecine, Université de Montréal, Montréal, Québec H3T 1J4, Canada
[d] Centre de Recherche de l'Hôpital Maisonneuve-Rosemont, Montréal, Québec H1T 2M4, Canada

ARTICLE INFO

Article history:
Received 3 December 2009
Accepted in revised form 25 March 2010
Available online xxx

Keywords:
low-coherence interferometry
eye kinematics
longitudinal movement

ABSTRACT

We demonstrate an optical instrument that can measure the axial displacement of different eye tissues, including the cornea and the fundus. The instrument is based on spectral-domain low-coherence interferometry, which extracts displacement information from sequential axial scans of the eye with 100 Hz sampling frequency and with a precision of 400 nm. Longitudinal retinal and corneal movements were successfully measured *in vivo* in live rats, and Fourier analysis of the signal revealed the signature of the respiratory and cardiac cycles at 1.0 and 3.5 Hz, respectively. The effective amplitudes of retinal and corneal displacements at the cardiac frequency were found to be about 1.10 and 1.37 μm, respectively. The synchrony and direction of these two movements relative to the systole and diastole were found to be nearly the same. This novel instrument can be applied to assess biomechanical properties of the eye, which could be important for early diagnosis and for understanding the pathophysiology of glaucoma and other ocular diseases.

1. Introduction

There is increasing evidence that the biomechanical properties of the eye may be involved in the development of glaucoma (Downs et al., 2008; Hommer et al., 2008; Lesk et al., 2006; Mangouritsas et al., 2009). For five decades, rigidity of the sclera or the lamina cribrosa has been invoked as contributing to the risk of open angle glaucoma (OAG) (Drance, 1960; Levy et al., 1981; Quigley and Addicks, 1981). Thinner corneas appear to be a risk factor for the development and progression of OAG (Gordon et al., 2002; Leske et al., 2007), and a thinner cornea was associated with a greater pressure-dependant mobility of the lamina cribrosa (Lesk et al., 2006). It is also known that the eye volume and intraocular pressure are pulsatile. The pulsatile nature of the eye has been described by Silver et al. (Silver and Farrell, 1994) as a result of an imbalance between pulsatile blood inflow and steady blood outflow into the elastic eye. Each bolus of blood entering the eye causes an increase in the volume of the contents of the globe with a consequent rise in intraocular pressure, and then a decrease in volume and pressure during the outflow process. This pulsatility drives the displacement of the various ocular tissues, while the amplitude of the movement necessarily depends on both the ocular hemodynamics and on the eye's biomechanical properties. It is not yet known whether the pulsatile movements of ocular tissues such as the lamina cribrosa could contribute to the pathophysiology of glaucoma, but if they do then their measurement could be used as an early diagnostic/prognostic test. Furthermore, as demonstrated by Hommer et al. (Hommer et al., 2008), measurement of the pulsatile movement of the eye can be used to estimate the ocular volume change, and thus the ocular rigidity from the Friedenwald equation (Friedenwald, 1937), which may lead to insights on the pathophysiology of glaucoma.

Various techniques for measuring pulsatile ocular movements have been reported in the literature. The contact techniques include plethysmography (Bosley et al., 1993), a variant of the Goldman's applanation tonometer (Krakau et al., 1995), and ultrasound transducers (Kowalska et al., 2008). However, for clinical measures, a non-contact technique is preferred. The non-contact methods are videokeratoscopy (Iskander and Kasprzak, 2006; Kasprzak and Iskander, 2007), laser and low-coherence interferometry (Dragostinoff et al., 2009; Fercher, 1984; Fercher et al., 1988; Schmetterer et al., 1995), and spectral-domain optical coherence tomography (SD-OCT) (Kasprzak et al., 2007), which are briefly

☆ M.L, MW and TO hold patents on the device described in this paper.
* Corresponding author.
E-mail address: ozaki@emt.inrs.ca (T. Ozaki).
[1] These authors contributed equally to this work.

0014-4835/$ – see front matter © 2010 Elsevier Ltd. All rights reserved.
doi:10.1016/j.exer.2010.03.022

described in the following. High-speed videokeratoscopy is based on imaging the reflection of concentric rings projected on the anterior cornea in order to measure the corneal topography. Due to its video-rate sampling, this technology also provides the ability to detect the displacement of the corneal apex. In addition to videokeratoscopy, all above-mentioned contact techniques, including plethysmography, variant of the Goldman tonometer, videokeratoscopy and ultrasound transducer, are limited to the measurement of corneal movements and cannot be applied to investigate the biomechanical properties of the eye's posterior structures, nor the whole globe. In laser interferometry technique, the eye is illuminated with a laser beam of high coherence length, which is reflected at the front surface of the cornea as well as at the retina. The reflected signals interfere with each other to produce an interference pattern which is recorded over time to extract the relative movement between cornea and retina, i.e. the ocular pulsation (Schmetterer et al., 1995). In this technique, movement of the retina and the cornea cannot be obtained independently, therefore no information about the direction of the movement of cornea or retina can be deduced. Also, as the laser source used in this technique has a high coherence length, it is difficult to determine with high certainty the eye element producing the interference pattern. The low-coherence interferometry technique is similar to the previous technique except that a broadband source with low-coherence length is used. Interference can be produced between the cornea and a specific layer of the retina, which allow the depth-resolved measurement of ocular fundus pulsations (Dragostinoff et al., 2009). Still, in this technique, pulsations of only one layer of the retina relative to cornea can be recorded, and the directionality of the movement cannot be recovered. Finally, in the SD-OCT technique cross-sectional images of the different eye elements are obtained from a series of laterally adjacent depth-scans. The depth-scans are obtained from the spectrally resolved interferogram obtained at the exit of an interferometer, which combines the low-coherent light reflected by a reference mirror and the sample eye. Video-rate imaging allows the extraction of the movement of individual eye tissues such as the cornea, the crystalline lens, and the retina (Kasprzak et al., 2007). This technology thus provides the ability to evaluate the biomechanical properties of individual eye elements.

To distinguish the various eye structures and to avoid aliasing of the data, the technique employed should at least provide axial resolution of 1 μm and sampling rate of 100 Hz. Videokeratoscopy was characterized with a resolution in displacement measurement of about 10 μm at 50 Hz (Kasprzak and Iskander, 2007). On the other hand, ultrasound transducers can resolve 2 μm at 100 Hz at the cornea (Kowalska et al., 2008), and SD-OCT 2 μm at 94 Hz (Kasprzak et al., 2007). Laser interferometry technique surpass all above-mentioned techniques, with a theoretical resolution of half the wavelength of the source (λ/2, where λ is the wavelength of the laser) and a sampling frequency up to 600 Hz (Dragostinoff et al., 2009).

In this paper, we demonstrate a novel non-invasive instrument based on spectral-domain low-coherence interferometry (SD-LCI), which extracts movement information from sequential axial scans. Our device was tested in the laboratory using model materials, as well as *in vivo* using live anesthetized rat. It resulted in better performance than most alternative methods, demonstrating a precision of approximately 400 nm at 100 Hz sampling frequency. Measurements on live animals using this newly developed equipment provided new elements for understanding of the ocular dynamics.

2. Theoretical background

Low-coherence interferometry (Fercher et al., 1995) is based on a Michelson interferometry, where a broadband light source is used to illuminate a reference surface and a sample (Fig. 1). The reflected

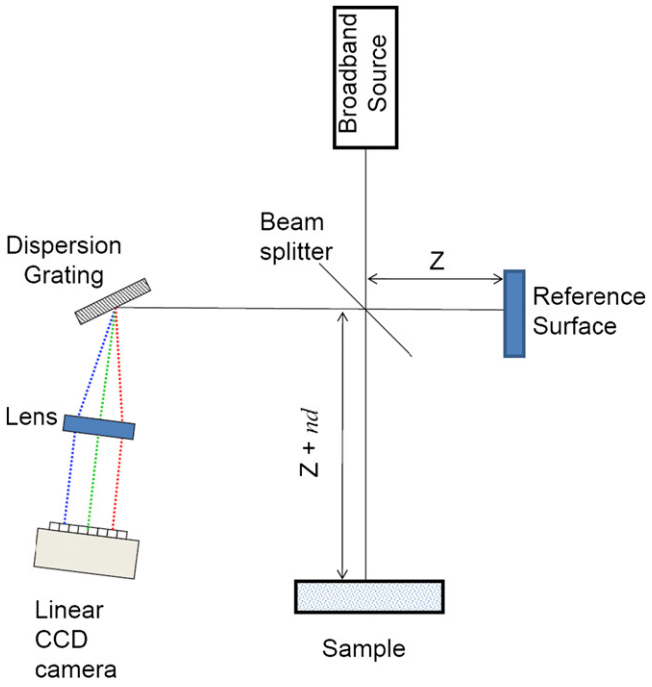

Fig. 1. Schematic diagram of a Fourier domain low-coherence interferometry system.

beams from sample and reference are recombined, producing interference. Using a diffraction grating that separates angularly the different wavelength components of the light, the spectrum of the interference signal can be observed using a linear CCD array (Fig. 1). The intensity distribution along the *k*-axis (wavenumber-axis) on the linear CCD camera, $I(K)$, can be described as the light source spectrum, $I_0(K)$, with a sinusoidal modulation at the exact frequency of the optical path difference (OPD). As the OPD is the product of the geometric length difference between both arms of the interferometer, d, and the index of refraction of the medium through which it propagates, n,

$$\mathrm{OPD} = 2nd \tag{1}$$

the spectrum intensity distribution along the *k*-axis can be written as

$$I(K) = I_0(K)(1 + \alpha\cos(2ndk + \phi)), \tag{2}$$

where α is a dimensionless parameter related to the visibility of interference fringes and φ is a phase constant.

In order to use the modulation frequency in the spectrum as a means to extract an accurate measurement of the geometric length, a Fourier transformation is performed on the spectrum. Assuming $I_0(K)$ has a Gaussian profile of bandwidth Δk, the Fourier transformation of Eq. (2) leads to an analytical solution of the form

$$I(x) \sim \alpha I_0(x - 2nd) + I_0(x), \tag{3}$$

where $I_0(x)$ is a Gaussian function of width equal to the coherence length of the source. From Eq. (3) it can be deduced that in the Fourier transformed space, the interference pattern has two peaks: a stationary peak centered at $x = 0$, revealing the light source spectrum, and a second peak of amplitude multiplied by the fringes visibility α, centered at $x = 2nd$. Thus, the center of this second peak is located at the OPD of the interferometer (neglecting the refractive index dependence on wavelength). In the case of samples composed of several partially reflective layers, successive peaks will be observed in the transformed space, and their centers will

Please cite this article in press as: Singh, K., et al., Development of a novel instrument to measure the pulsatile movement of ocular tissues, Exp. Eye. Res. (2010), doi:10.1016/j.exer.2010.03.022

provide the exact corresponding location with respect to the reference sample. The Fourier transformation of the spectrum obtained on the CCD providing the reflectivity profile as a function of depth is commonly called an axial scan (A-scan), or depth scan.

The maximum geometrical length difference (d_{max}) that can be measured following this methodology is limited by Nyquist criterion. The highest spectrum modulation frequency that the CCD can sample avoiding aliasing corresponds to d_{max}, i.e. the high frequency limit after the FFT algorithm. This distance is called the depth range (Wojtkowski et al., 2004) and is given by:

$$d_{max} = \frac{\ln 2}{\Delta k} N, \tag{4}$$

where Δk is the bandwidth of the light source in k-space, and N is the number of pixel of the linear CCD camera.

The longitudinal resolution in SD-LCI, defined as the minimum distance between two layers of the sample such that they can be identified separately, is inversely proportional to the bandwidth of the light source and is given by (for a light source with Gaussian shape) (Izatt et al., 1996; Wojtkowski et al., 2004)

$$\Delta d = \frac{4 \ln 2}{\Delta k}. \tag{5}$$

The longitudinal resolution also corresponds to the coherence length of the source.

3. Experimental details

3.1. Experimental set-up and methods

We show in Fig. 2 a schematic diagram of the optical set-up for the SD-LCI, which was used in this work to measure the retina and cornea position. A fiber-based Michelson interferometer is used with a superluminescent diode (SLD, Superlum) that has a central wavelength of 844 nm and a bandwidth of 46 nm. According to Eq. (5), this source can theoretically provide a longitudinal resolution of ~7 μm in air. The light was split using a 2 × 2, 80:20 fiber coupler into the reference and sample arms terminated with fiber collimators. At the reference arm, the light was reflected by a broadband mirror placed on a motorized translation stage (PI Instrument). The reference arm beam was attenuated by a neutral density filter (NDF) in order to keep its total intensity below the saturation level of the detector. The sample arm was coupled to a fundus camera, which comprised a CCD camera (Pulnix), a white light source and an imaging lens (focal length $f = 52$ mm). In addition, two lenses ($f = 46$ mm and $f = 33$ mm) were used in front of the sample to correct for myopia or hypermetropia of the eye. The collimated sample beam was focused by the crystalline lens on to the fundus, or by a focusing lens ($f = 46$ mm) onto the cornea. The SLD power incident onto the eye was 700 μW, which is safe for continuous illumination of the human eye according to ANSI safety standards (Delori et al., 2007). The two reflected beams (one reflected from the eye layer of interest and the other from the reference mirror) were recombined in the fiber coupler, then dispersed using a diffraction grating (1200 lines/mm) and focused by a lens ($f = 150$ mm) on to a linear CCD camera (CCD 1000, Gerhard Stresing). The camera exposure time was set to 400 μs. The full SLD spectrum spanned 700 pixels on the linear CCD camera, which allowed, according to Eq. (4), a theoretical depth range of ~1.2 mm in air. The measured sensitivity close to the zero delay position was found to be 72 dB with a decay of 35 dB as one approached 80% of the maximal depth range. The signal from the linear CCD camera was processed using a 2.0 GHz computer using custom software (LabView; National Instruments Inc.).

To establish a relationship between the eye movements and the cardiac pulsations, heartbeats were simultaneously recorded using a custom-made oximeter (Wukitsch et al., 1987). For both cornea and retina recordings, the oximeter was located at the exact same position, i.e. at the tail of the rat. The oximeter used an infrared light-emitting diode and a photodiode connected to an amplification circuit that was digitized with the computer. Overall, the total data acquisition time of the CCD camera and oximeter signals provided a sampling rate of 100 Hz. Interference spectra and oximeter signal were recorded during series of 5 s.

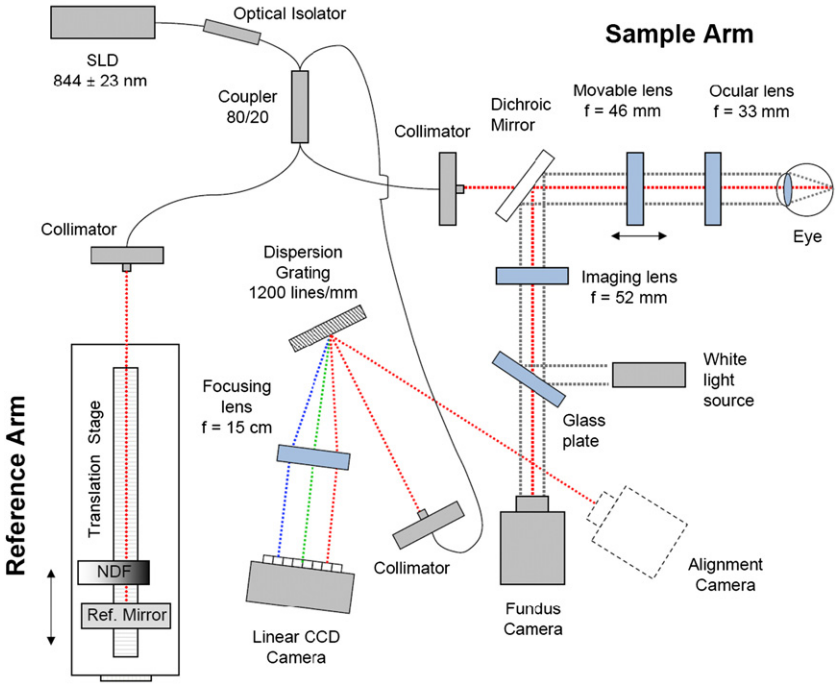

Fig. 2. Schematic diagram of the optical set-up of the SD-LCI system.

Please cite this article in press as: Singh, K., et al., Development of a novel instrument to measure the pulsatile movement of ocular tissues, Exp. Eye. Res. (2010), doi:10.1016/j.exer.2010.03.022

Post data processing involved Fourier analysis and peak tracking over the sequential axial scan. By tracking the position of the maximum peak value, the displacement resolution, i.e. the minimum change in the position that can be measured, is determined by the position increment between two points of the axial scan, which depends on the light source bandwidth and the total number of pixels of the camera, in our case yielding a displacement resolution of 3.6 μm. Nevertheless, the position of a layer can be extracted with much higher resolution by locating the central position of the Fast Fourier Transform (FFT) peak from curve fitting results (Costantino et al., 2003). Accordingly, central position of the FFT peak was calculated using the relation

$$\frac{\sum X_n I_n}{\sum I_n}, \tag{6}$$

where X is the position, I is the intensity and n is the index of the nth point in the FFT spectrum. Finally, in order to retrieve the amplitude of the displacement due to the cardiac rhythm, the recovered movement was filtered using the oximeter signal as a reference.

3.2. Accuracy, resolution, and precision

The displacement accuracy, resolution and precision of the SD-LCI was evaluated by tracking the peak center in the axial scan produced by a sample mirror placed on a piezoelectric stage (Piezosystem Jena), which itself was fixed on a motorized translation stage (PI Instrument). A typical axial scan of the sample mirror is shown in Fig. 3a, where the intense peak was attributed to the air/mirror interface.

The accuracy of the system, i.e. the degree of correctness of the measure, depends on the calibration of the instrument. We calibrated our SD-LCI by measuring the position of the peak in the axial scan as a function of the position of the translation stage, repeating this measurement at 100 μm intervals. With a position precision of 1 μm, the calibration can be obtained with 10^{-4} accuracy.

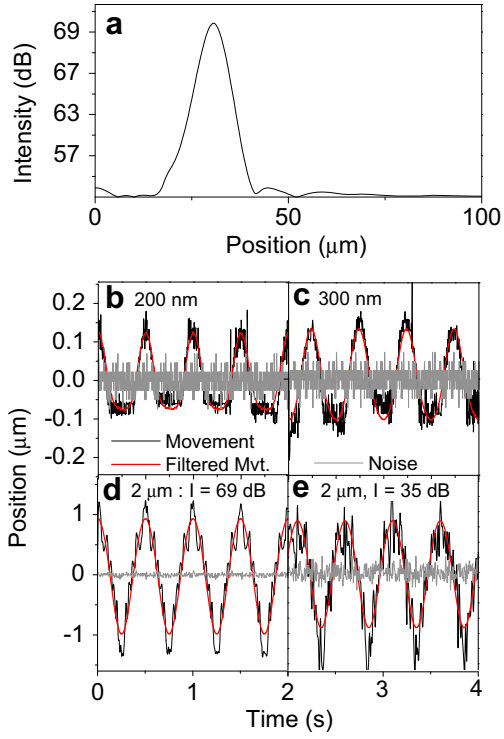

Fig. 3. (a) A-scan produced by the interference between the two surfaces of a microscope cover slip. Position as a function of time as recorded by the SD-LCI for a sample mirror placed on a piezoelectric stage moving with an amplitude of (b) 200 nm and (c) 300 nm. Position as a function of time for a sample mirror moving with an amplitude of 2 μm for signal intensity of (d) 69 dB and (e) 35 dB.

The displacement resolution (i.e. the smallest displacement increment that can be resolved) and precision (i.e. the reproducibility of the measurement) were verified by inducing a periodic movement to the mirror sample using a piezoelectric crystal, which had a characteristic movement resolution of 0.9 nm. The voltage applied to the piezoelectric stage was used as a reference signal for filtering. Fig. 3b and c show the measured positions of the sample mirror as a function of time for increasing movement amplitude. In these figures, negative (positive) positions correspond to movement in the forward (backward) direction relative to the sample surface position. By optimizing the interference contrast, a minimum displacement resolution of 100 nm could be measured. The precision of the system was verified by repeating the alignment of the system and using different illumination conditions. Fig. 3d and e show the position as a function of time for a sample mirror moving with an amplitude of 2 μm for a signal intensity of 69 dB (Fig. 3d) and 35 dB (Fig. 3d), which corresponds to the maximal intensity and the intensity close to actual *in vivo* experiment with animals. The difference in the displacement amplitude between the two illumination conditions is of the order of 400 nm. Thus, it is safe to conclude that the SD-LCI can measure a displacement with a precision of 400 nm.

3.3. Animal manipulations

The rats were anesthetized with intraperitoneal injections of ketamine and xylazine mixture (0.1 mL per 100 g body weight). After anesthesia, animals were placed on a custom-made fixation platform that allowed three axes of rotation which facilitated careful alignment of the eye and the sample beam. All animal handlings were performed under protocols compliant with the Canadian Council on Animal Care with the approval of the Animal Care and Use Committee at the Hospital Maisonneuve-Rosemont.

4. Results

The SD-LCI developed was used to measure the longitudinal movement of the retina and cornea in live rats. To measure retinal movements, the experimental set-up shown in Fig. 2 was used, and a collimated sample beam was focused on to the fundus by the eye. A typical axial profile of the retinal layers is shown in Fig. 4a. The multiple lines were assigned to the various retinal tissue layers after comparing them with the OCT images available in the literature (Srinivasan et al., 2006). The retinal tissue layers that can be seen in the A-Scan are nerve fiber layer (NFL), outer nuclear layer (ONL), photoreceptor's inner segment (PR-IS), photoreceptor's outer segment (PR-OS), retinal pigment epithelium (RPE) and choroid (CH). For each scan, the central position of the FFT spectrum was precisely determined using the fitting method described above. The geometric position of the retina was determined from Eq. (1) using the average refractive index of 1.415 for the rat eye (Remtulla and Hallett, 1985; Schmucker and Schaeffel, 2004).

For measuring the corneal displacement, the set-up shown in Fig. 2 was used without an ocular lens, so that the sample beam was directly focused on to the cornea. A typical axial profile of the cornea is shown in Fig. 4b, where the intense peak observed is attributed to the air/cornea interface. The peak near the zero position can be attributed to auto-interference within the sample, as this peak does not change in position when the reference mirror is moved. The last visible peak is the second harmonic of the air/cornea peak. The position of the air/cornea peak was also determined using the

Please cite this article in press as: Singh, K., et al., Development of a novel instrument to measure the pulsatile movement of ocular tissues, Exp. Eye. Res. (2010), doi:10.1016/j.exer.2010.03.022

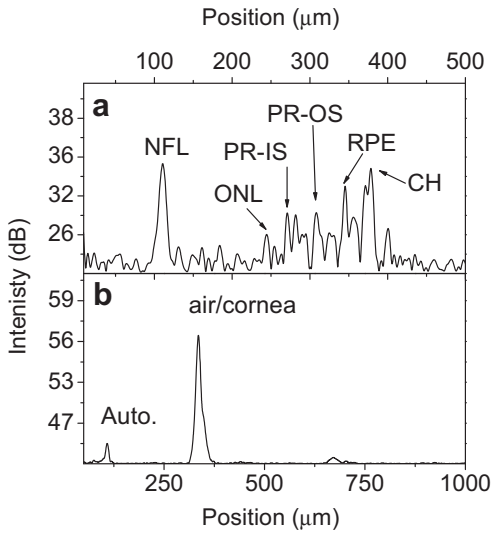

Fig. 4. A-scan of (a) the retina and (b) the cornea in a live anesthetized rat.

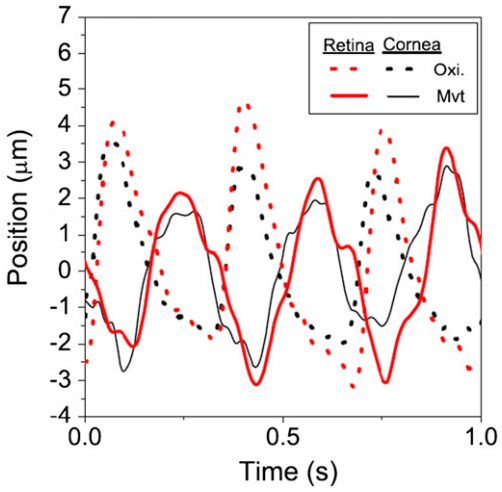

Fig. 6. Filtered movement of the retina and the cornea, along with their respective oximeter signal which were matched for comparison.

fitting method, and sequential recordings were obtained to extract the movement.

The displacements obtained using the procedure described above are shown in Fig. 5a and b for the retina and the cornea, respectively. To investigate the spectral components of such displacements, FFT was performed on the data, whose results are shown in Fig. 5c and d. Two main frequency components are present in the retinal and corneal movements: one at 1.0 Hz, which is due to respiration, and the other at 3.5 Hz, which is due to cardiovascular rhythm. To confirm the latter, the FFT of the oximeter signal is also plotted in Fig. 5c and d, which also reveals a frequency at 3.5 Hz.

To retrieve the relative movement of the retina and the cornea induced by the blood pulsatility, the oximeter signal was used as a common clock. These movements are shown along with the oximeter signals in Fig. 6. We shall recall that corneal and retinal movements were recorded at different times. Therefore, the reference oximeter signals were matched to compare the two movements. One can see in Fig. 6 that, for a similar oximeter signal, the retinal and the corneal movement of the eye are nearly in phase. As a result, we can conclude that the direction of the movement is the same for both tissues; during systole, the layers are pushed forward, whereas during diastole, the layers move backward.

For both tissues, the peak-to-peak amplitude was estimated over 30 cycles by locating the two extreme positions (maximum and minimum peaks) for every cycle. The mean of the peak-to-peak values are (3.7 ± 0.6) μm and (3.1 ± 0.7) μm for the retina and cornea, respectively, where the error corresponds to the standard deviation of the data. In order to compare our measurements with the literature (Kasprzak et al., 2007; Kowalska et al., 2009), we also calculated the effective amplitude of the movements, defined as the root-mean-square amplitude of the movement. The effective amplitude of the retinal and corneal movements due to cardiac pulsation is measured to be 1.10 and 1.37 μm, respectively.

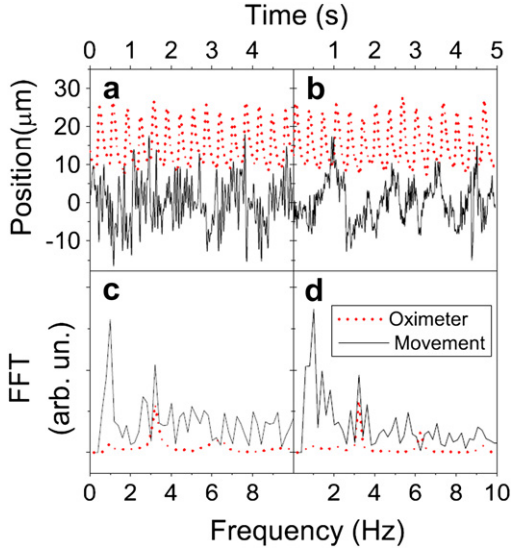

Fig. 5. Recorded movement of (a) the retina and (b) the cornea, and their corresponding FFT in (c) and (d), along with the oximeter signal and its FFT.

5. Discussion

Longitudinal retinal and corneal displacements were successfully measured with an SD-LCI annexed with an oximeter, working at an acquisition speed of 100 Hz with displacement precision of 400 nm. This instrument is a significant improvement in terms of the precision and acquisition speed, compared with previous works (Iskander and Kasprzak, 2006; Kasprzak et al., 2007). Along with these works, the results presented in this study show a correlation between the kinematics of eye and the cardiovascular system.

Further, this work provides a new finding in understanding the ocular hemodynamics. Since the oximeter signal can be used as an external reference, the retinal and corneal movements can be compared directly. It is clear from our results that the direction of the retinal and corneal movement relative to the systole and diastole is the same, and the phase of the two movements are similar. Therefore, our results show that with every heartbeat, the retina and cornea are both moving together, forward and backward. Our results thus provide elements of answer to the hypothesis formulated by Kasprzak et al. (Iskander and Kasprzak, 2006; Kasprzak and Iskander, 2007) from videokeratoscopy results, which mentioned that the cornea and the retina were either moving in the same or the opposite direction. Based on our results,

Please cite this article in press as: Singh, K., et al., Development of a novel instrument to measure the pulsatile movement of ocular tissues, Exp. Eye. Res. (2010), doi:10.1016/j.exer.2010.03.022

we can certainly confirm that cornea and retina are moving in the same direction. This process can be understood as follow. When the choroid is filled with blood during systole, the retina is pushed inward (towards the vitreous), which in turn induce a pulse in the vitreous humour that propagates towards the cornea to push it outward. Thus, both the cornea and the retina move in the same direction as a result of the blood flow into the eye. This way, the eye, as a whole, is moving forward during systole. However, the retina and the cornea could possibly be moving with different amplitudes because of different biomechanical properties, thus generating the ocular pulsation.

However, we should be careful in concluding on the eye deformation or pulsation from our current measurements. Because measurements are made at different time points, the present system only allows the measurement of the mean ocular pulsation using the mean movement amplitude of each individual layer. In the present experiment, we have found mean peak-to-peak amplitudes of (3.7 ± 0.6) μm and (3.1 ± 0.7) μm for the retina and cornea, respectively, which are essentially identical considering the standard deviation of the data. Furthermore, the effective amplitudes of 1.10 μm and 1.36 μm found respectively for the retina and cornea do not show significant differences, considering the standard deviation of the data and the precision of our instrument (400 nm). Therefore, we cannot conclude on the rat eye deformation from the experiment achieved with our system. Nevertheless, as the ocular pulsatility in humans was found to be about 2 μm (Dragostinoff et al., 2009), we expect the SD-LCI system to be easily able to measure it in humans with a precision of 400 nm. In human experiments, the use of anesthetics should not be necessary and eye alignment should be achieved with the help of a fixation point. Nevertheless, involuntary head and eye movement are expected. Still, we shall recall that movements that are occurring at frequencies different from that of the heart beating can be removed by filtering the movements using oximeter signal as a gate filter in the frequency domain.

We should also note that the current equipment requires two different measurements (one at the retina, and the other at the cornea) that are performed at different times. Therefore, this could also complicate the understanding of the exact relationship between the two movements. It would be of great interest to modify the SD-LCI and measure simultaneously the retinal and corneal movement. In addition to the phase of the relative movement between the retina and the cornea, this revised equipment could also be used to determine the magnitude of the ocular pulse. As such, the SD-OCT technique is promising for measuring ocular pulsation, but further improvement is necessary.

In conclusion, better understanding of the kinematics of the eye displacement and deformation could provide some new insights on eye diseases related to ocular pulsatility. Our study has shown that the SD-LCI has the sensitivity and acquisition speed required to measure the longitudinal movements of ocular tissues, such as the retina and cornea. Thus, the instrument demonstrated in this paper could pave the way to future research and diagnostic methods for eye diseases, such as glaucoma.

Acknowledgments

The authors acknowledge support from the Ministère du Développement Économique de l'Innovation et de l'Exportation du Québec, the Fonds Québécois de la Recherche sur la Nature et les Technologies, the Fonds de la Recherche en Santé du Québec, the Natural Sciences and Engineering Research Council of Canada, and the Canadian Institute for Photonic Innovations. The authors also acknowledge Dr. Leo Schmetterer for his helpful discussions.

References

Bosley, T., Cohen, M., Gee, W., Reed 3rd, J., Sergott, R., Savino, P., 1993. Amplitude of the ocular pneumoplethysmography waveform is correlated with cardiac output. Stroke 24, 6–9.
Costantino, S., Martinez, O.E., Torga, J.R., 2003. Wide band interferometry for thickness measurement. Optics Express 11, 952–957.
Delori, F.C., Webb, R.H., Sliney, D.H., 2007. Maximum permissible exposures for ocular safety (ANSI 2000), with emphasis on ophthalmic devices. J. Opt. Soc. Am. A-Opt. Image Sci. Vis. 24, 1250–1265.
Downs, J.C.P., Roberts, M.D.P., Burgoyne, C.F.M., 2008. Mechanical environment of the optic nerve head in glaucoma. Optom.Vis. Sci. 85, E425–E435.
Dragostinoff, N., Werkmeister, R.M., Groschl, M., Schmetterer, L., 2009. Depth-resolved measurement of ocular fundus pulsations by low-coherence tissue interferometry. J. Biomed. Opt. 14, 054047.
Drance, S.M., 1960. The coefficient of Scleral rigidity in normal and glaucomatous eyes. AMA Arch. Ophthalmol. 63, 668–674.
Fercher, A.F., Mengedoht, K., Werner, W., 1988. Eye-length measurement by interferometry with partially coherent light. Optics Lett. 13, 186–188.
Fercher, A.F., Hitzenberger, C.K., Kamp, G., El-Zaiat, S.Y., 1995. Measurement of intraocular distances by backscattering spectral interferometry. Opt. Commun. 117, 43–48.
Fercher, A.F., 1984. Invivo measurement of fundus pulsations by laser interferometry. IEEE J. Quantum Electron. 20, 1469–1471.
Friedenwald, J., 1937. Contribution to the theory and practice of tonometry. Am. J. Ophthalmol. 20, 985–1024.
Gordon, M.O., Beiser, J.A., Brandt, J.D., et al., 2002. The ocular hypertension treatment study – baseline factors that predict the onset of primary open-angle glaucoma. Arch. Ophthalmol. 120, 714–720.
Hommer, A., Fuchsjager-Mayrl, G., Resch, H., Vass, C., Garhofer, G., Schmetterer, L., 2008. Estimation of ocular rigidity based on measurement of pulse amplitude using pneumotonometry and fundus pulse using laser interferometry in glaucoma. Invest. Ophthalmol. Vis. Sci. 49, 4046–4050.
Iskander, D.R., Kasprzak, H.T., 2006. Dynamics in longitudinal eye movements and corneal shape. Ophthal. Physl. Opt. 26, 572–579.
Izatt, J.A., Kulkarni, M.D., Wang, H.-W., Kobayashi, K., Sivak Jr., M.V., 1996. Optical coherence tomography and microscopy in gastrointenstinal tissues. IEEE J. of Sel. Top. Quant. Electron. 2, 1017–1028.
Kasprzak, H.T., Iskander, D.R., 2007. Spectral characteristics of longitudinal corneal apex velocities and their relation to the cardiopulmonary system. Eye 21, 1212–1219.
Kasprzak, H., Iskander, D.R., Bajraszewski, T., Kowalczyk, A., Nowak-Szczepanowska, W., 2007. High accuracy measurement of spectral characteristics of movements of the eye elements. Optica. Pura. Y Aplicada. 70, 7–11.
Kowalska, M.A., Kasprzak, H.T., Iskander, D.R., 2008. Ultrasonic measurement of binocular longitudinal corneal apex movements and their correlation to cardiopulmonary system. Biocybern. Biomed. Eng. 28, 35–43.
Kowalska, M.A., Kasprzak, H.T., Iskander, D.R., 2009. Comparison of high-speed videokeratoscopy and ultrasound distance sensing for measuring the longitudinal corneal apex movements. Ophthal. Physl. Opt. 29, 227–234.
Krakau, C.E.T., Lindberg, S., Havelius, U., 1995. An instrument for recording the ocular pulse wave. Acta Ophthalmologica Scandinavica 73, 472–474.
Lesk, M.R., Hafez, A.S., Descovich, D., 2006. Relationship between central corneal thickness and changes of optic nerve head topography and blood flow after intraocular pressure reduction in open-angle glaucoma and ocular hypertension. Arch. Ophthalmol. 124, 1568–1572.
Leske, M.C., Heijl, A., Hyman, L., Bengtsson, B., Dong, L., Yang, Z., 2007. Predictors of long-term progression in the early manifest glaucoma trial. Ophthalmology 114, 1965–1972.
Levy, N.S., Crapps, E.E., Bonney, R.C., 1981. Displacement of the optic nerve head – response to acute intraocular pressure elevation in primate eyes. Arch. Ophthalmol. 99, 2166–2174.
Mangouritsas, G., Morphis, G., Mourtzoukos, S., Feretis, E., 2009. Association between corneal hysteresis and central corneal thickness in glaucomatous and non-glaucomatous eyes. Acta Ophthalmologica 87, 901–905.
Quigley, H.A., Addicks, E.M., 1981. Regional differences in the structure of the lamina cribrosa and their relation to glaucomatous optic nerve Damage. Arch. Ophthalmol. 99, 137–143.
Remtulla, S., Hallett, P.E., 1985. A schematic eye for the mouse, and comparisons with the rat. Vision Research 25, 21–31.
Schmetterer, L.F., Lexer, F., Unfried, C.J., Sattmann, H., Fercher, A.F., 1995. Topical measurement of fundus pulsations. Optical Engineering 34, 711–716.
Schmucker, C., Schaeffel, F., 2004. A paraxial schematic eye model for the growing C57BL/6 mouse. Vision Research 44, 1857–1867.
Silver, D.M., Farrell, R.A., 1994. Validity of pulsatile ocular blood flow measurements. Surv. Ophthalmol. 38 (Suppl), S72–S80.
Srinivasan, V.J., Ko, T.H., Wojtkowski, M., et al., 2006. Noninvasive volumetric imaging and morphometry of the rodent retina with high-speed, ultrahigh-resolution optical coherence tomography. Invest. Ophthalmol. Vis. Sci. 47, 5522–5528.
Wojtkowski, M., Srinivasan, V.J., Ko, T.H., Fujimoto, J.G., Kowalczyk, A., Duker, J.S., 2004. Ultrahigh-resolution, high-speed, Fourier domain optical coherence tomography and methods for dispersion compensation. Optics Express. 12, 2404–2422.
Wukitsch, M.W., Petterson, M.T., Tobler, D.R., Pologe, J.A., 1987. Pulse oximetry: analysis of theory, technology, and practice. J. Clin. Monit. Comput. 4, 290–301.

Please cite this article in press as: Singh, K., et al., Development of a novel instrument to measure the pulsatile movement of ocular tissues, Exp. Eye. Res. (2010), doi:10.1016/j.exer.2010.03.022